SUPPORTING INFORMATION

InGaN Quantum Dots Studied by Correlative Microscopy Techniques for Enhanced Light-Emitting Diodes

Ioanna Dimkou,[*,†] Enrico Di Russo,[†,⊥] Pradip Dalapati,[‡,¶] Jonathan Houard,[‡] Nevine Rochat,[†] David Cooper,[†] Edith Bellet-Amarlic,[§] Adeline Grenier,[†] Eva Monroy,[§] and Lorenzo Rigutti[‡]

[†] Univ. Grenoble Alpes, CEA, LETI, F-38000 Grenoble, France

[‡] UNIROUEN, CNRS, Groupe de Physique des Matériaux, Normandie Université, 76000 Rouen, France

[§] Univ. Grenoble-Alpes, CEA, IRIG-PHELIQS, 38000 Grenoble, France

* Corresponding Author: ioanna.dimkou@cea.fr

ATOMIC FORCE MICROSCOPY

Figure S1 presents a 0.7×0.7 μm^2 atomic force microscopy (AFM) scan of the topmost uncapped InGaN quantum dots (QDs) layer. The measurement was performed using a Bruker AFM operated in the tapping mode, with a TESPA-V2 tip. Let us remind that the growth was abruptly stopped just after the deposition of the last InGaN QD layer, and the substrate temperature was rapidly decreased to preserve the surface. From the image, the QD density is ≈ 5×10^{11} cm^{-2} and the QD height (above the wetting layer) is 0.9±0.2 nm. This value and its error bar are extracted by measurement of the peak-to-peak height profiles of around 15 well-identified QDs in figure S1, and validated by a similar analysis in a second image in another area of the sample. The measurement is extracted manually from height profiles.

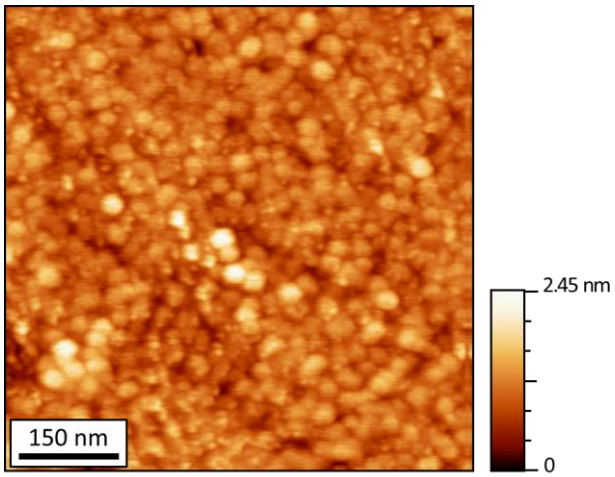

Figure S1. AFM scan of the InGaN/GaN QD sample under study.

The measurements of QD height and diameter by AFM are influenced by the probe tip shape. This is particularly important when the topography varies sharply (large slope) or in the case of close-packed nanostructures, since the tip may not penetrate between the objects. Here we estimate the errors that

we might accumulate in the case of measuring faceted islands, considering the two extreme situations: well-separated and close-packed islands, as described in figures S2(a) and (b), respectively.

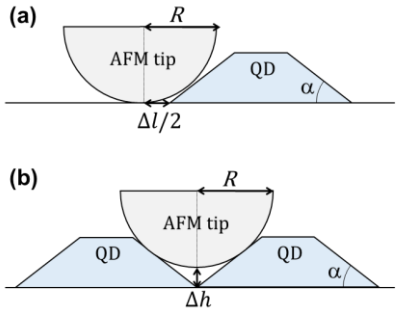

Figure S2. Schematic description of the errors associated to the AFM measurement of faceted islands in the case of (a) well-separated and (b) close-packed islands.

In the case of well-separated islands [figure S2(a)], the measurement of the height is precise, but the measurement of the diameter is larger by Δl, with

$$\Delta l = 2R\left(\frac{1-\cos\alpha}{\sin\alpha}\right) \quad \text{(S1)}$$

If we consider that the radius of the TESPA-V2 tips is 7 nm and the commonly observed faceting of III-nitride QDs is {10-13}, forming an angle $\alpha \approx 30°$ with the growing surface, the expected error would be Δl = 3.8 nm.

In the case of close-packed QDs, the measurement of the QD diameter would be correct, but the tip would not be able to reach the wetting layer between two QDs [see figure S2(b)]. The associated error in the measurement of the QD height is

$$\Delta h = -R\left(\frac{1-\cos\alpha}{\cos\alpha}\right) \quad \text{(S2)}$$

For a tip with R = 7 nm and QDs with $\alpha \approx 30°$, the expected error is Δh = –1.1 nm.

Looking back at figure S1, the QD ensemble is dense, which makes it difficult to identify if the configuration is closer to figure S2(a) or S2(b) without supporting information from another characterization technique. Analyzing height profiles of figure S1, the distance between QDs is in the range of 20-40 nm. However, transmission electron microscopy (TEM) images of the sample (shown below) suggest a QD diameter in the range of 12-17 nm, and a typical in-plane diameter of 15.4±1.4 nm is extracted from atom probe tomography (APT) measurements, as described in the body of the paper. Therefore, comparing these results, we conclude that the QDs are far enough to obtain a reliable measurement of the height, with an overestimation of the QD base diameter.

TRANSMISSION ELECTRON MICROSCOPY

High-angle annular dark field (HAADF) and high-resolution bright field (BF) scanning transmission electron microscopy (STEM) images of the InGaN/GaN QD superlattice viewed along <11-20> are displayed in figure S3. The wetting layer is not well defined due to the high density of dots with a diameter smaller than the thickness of the lamella specimen (70±10 nm), which results in more than one dot being projected in the images. It is nevertheless possible to measure with atomic precision the height of the QD layer (including wetting layer), which is 8±1 monolayers (ML), i.e. 2.0±0.3 nm. The diameter of the QDs, estimated from the variations of contrast in the images, would be in the range of 12-17 nm.

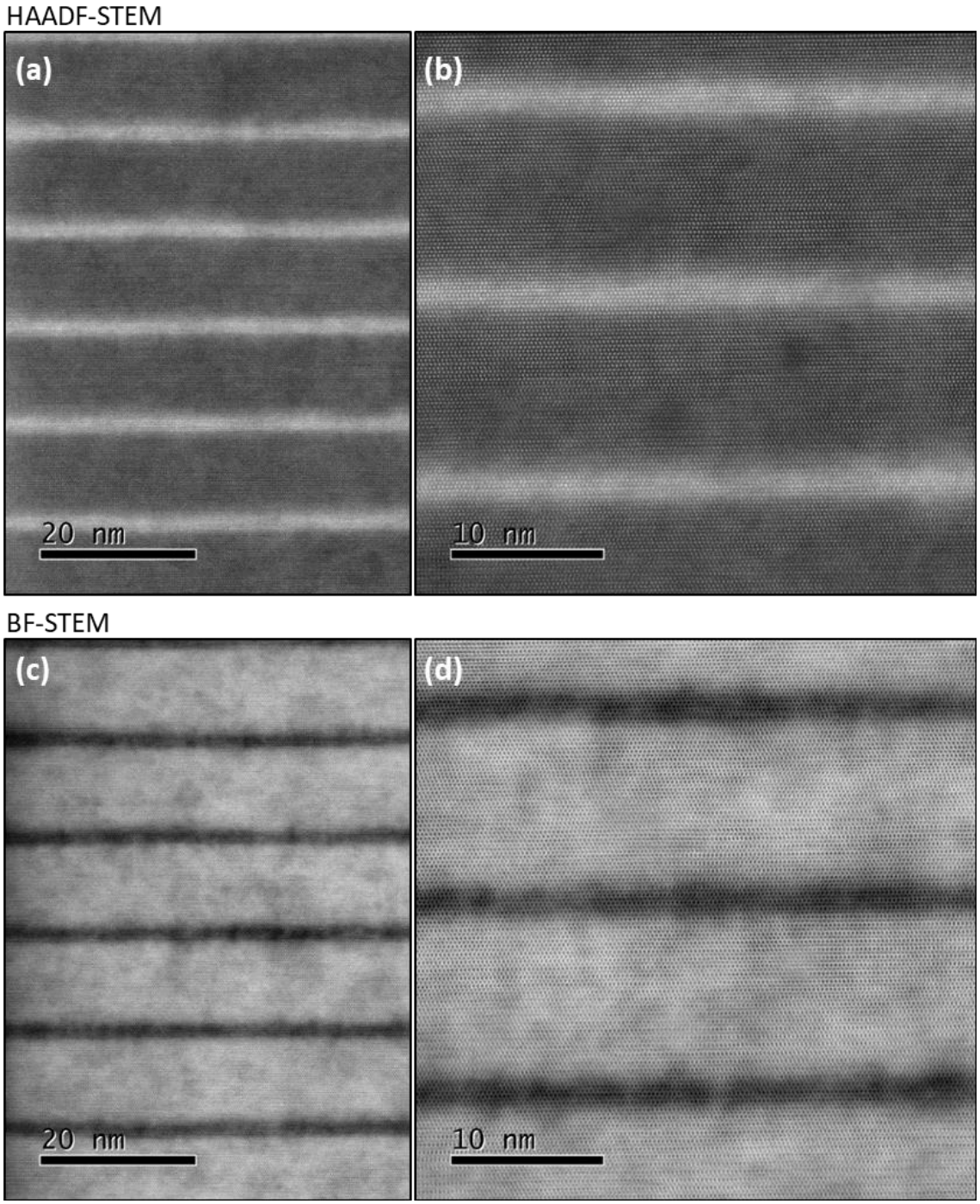

Figure S3. Cross-section (a,b) HAADF and (c,d) BF-STEM images of the InGaN/GaN QD superlattice viewed along the <11-20> zone axis.

VARIATION OF THE CATHODOLUMINESCENCE ALONG THE GROWTH AXIS

Figure S4 presents (a) a panchromatic cross-section CL mapping of a cleaved edge of the as-grown sample, and (b) CL spectra extracted at various points of (a), moving from the interface between the GaN and the InGaN QD superlattice (1) to the surface of the sample (6). The spectra recorded close to the interface present a narrow emission line at 355 nm, characteristic of GaN, and a broad emission that peaks at 317-319 nm, which is assigned to the QDs. In (a), the area where the GaN line is dominant is colored green and the area dominated by the QD emission is colored red. The spectral shift of the QD luminescence along the structure remains smaller than 2 nm, which is much smaller

than the emission linewidth (≈ 20 nm) and of the order of the spectral resolution of the spectrometer (±0.8 nm).

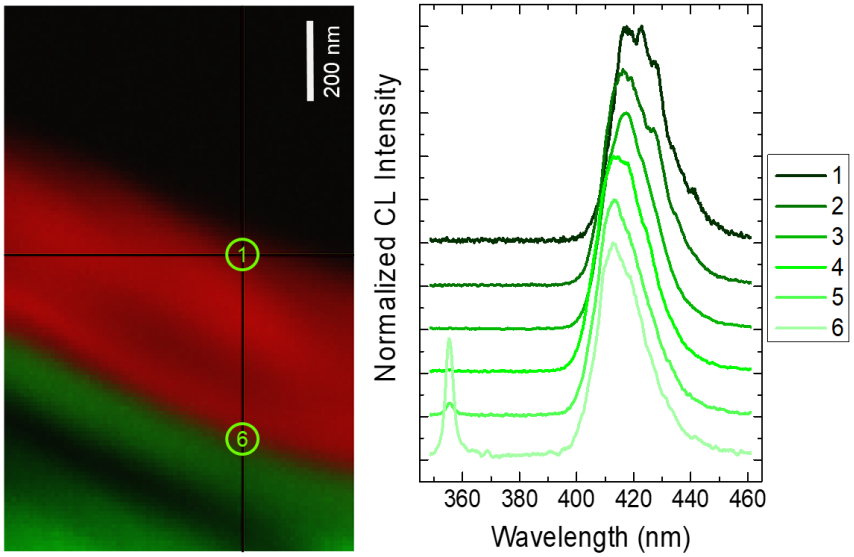

Figure S4. (a) Cross-section CL mapping of the as-grown structure, measured at 8 K. The area where the GaN emission (line at 355 nm) is dominant appears in green, and the area where the InGaN QD emission is dominant (417-419 nm) appears in red. (b) CL spectra measured at extracted at points of (a), moving from the GaN/InGaN interface (1) to the surface (6).

A similar CL study in the case of an APT specimen is displayed in figure S5, where (a) is a panchromatic CL mapping of it, and (b) presents CL spectra extracted by integrating slices of (a) moving from the interface between the GaN and the InGaN QD superlattice (1) to the specimen apex (7). Again, the spectra recorded close to the interface present a narrow emission line at 355 nm, characteristic of GaN, and a broad emission that peaks at 417-419 nm, which is assigned to the QDs. In (a), the area where the GaN line is dominant is colored green and the area dominated by the QD emission is colored red. The spectral shift of the QD luminescence along the structure remains smaller than 2 nm (without clear trend as a function of the location), which is much smaller than the emission linewidth (≈ 20 nm).

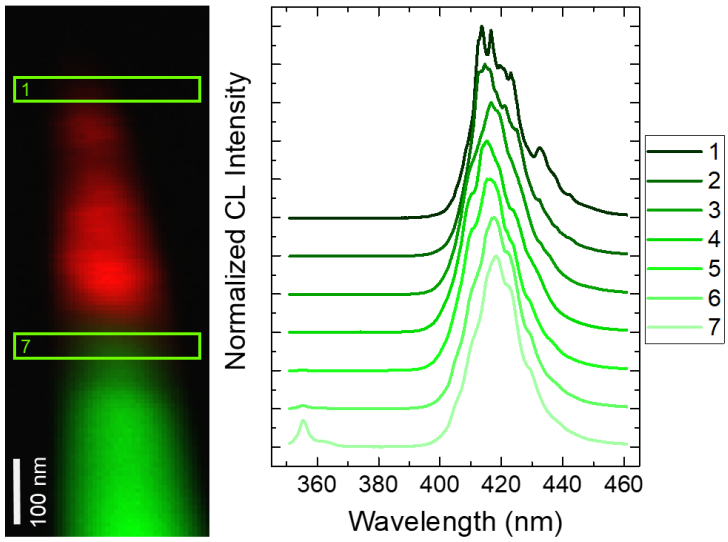

Figure S5. (a) CL mapping of the APT specimen, measured at 8 K. The area where the GaN emission (line at 355 nm) is dominant appears in green, and the area where the InGaN QD emission is dominant (417-419 nm)

appears in red. (b) CL spectra measured at extracted from different areas of (a), moving from the GaN/InGaN interface (1) to the apex (7).

MICROPHOTOLUMINESCENCE COUPLED WITH ATOM PROBE TOMOGRAPHY

Figure S6(a) shows micro-photoluminescence (µPL) spectra recorded *in-situ* during the laser-assisted atom probe tomography (La-APT) characterization of InGaN/GaN QDs at 80 K. Tip contained 15 QDs layers and we selected spectra that were recorded during the evaporation of each GaN barrier. The peak at 358 nm is related to the carrier recombination in the GaN buffer, whereas the broad band at around 415 nm is assigned to carrier recombination in the InGaN QDs. Figure S6(b) displays the APT reconstruction of the APT specimen obtained simultaneously with the µPL measurements.

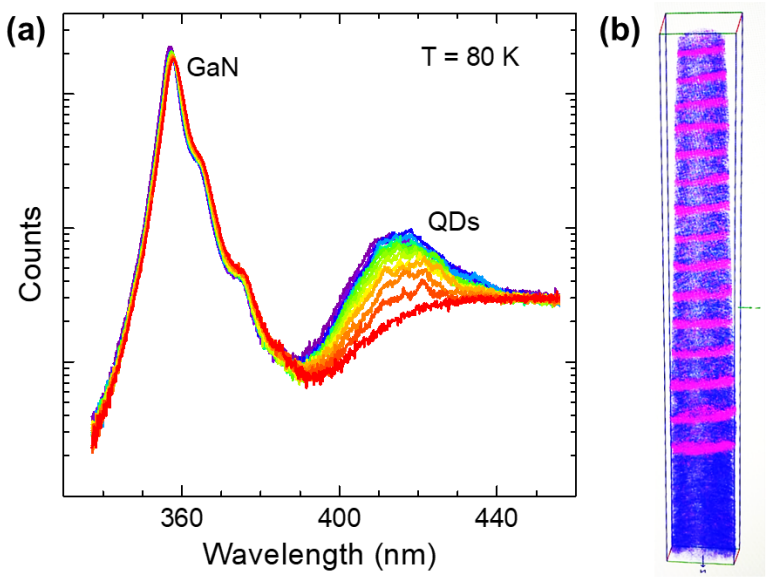

Figure S6. (a) Evolution of the µPL spectrum during the evaporation of the APT specimen. The spectra represented in the figure were recorded during the evaporation of each barrier. (b) 3D reconstruction of the In atom distribution in the analysed sample. The APT experiment was performed simultaneously with the µPL measurements. Ga atoms are represented in blue and In atoms are represented in magenta.

CALCULATION OF THE STRAIN DISTRIBUTION IN THE QDs

Figure S7 shows the distribution of the (a) in-plane (ε_{xx}) and (b) out-of-plane (ε_{zz}) strain in two InGaN QDs in the center of the QD stack. The simulation process is described in the Methods. The geometry and indium distribution in the simulated structure corresponds to the nominal values, illustrated in figure 7(a). As expected, the in-plane lattice is compressed, and the out-of-plane lattice is expanded. However, the out of plane deformation is significantly smaller than expected in the case of biaxial strain. This is clearly visible in the image, where the value of ε_{zz} inside the QDs is significantly smaller (yellow-orange) than its value in the wetting layer (red), in spite of the higher indium content in the dots (13%) with respect to the wetting layer (6%). The difference is due to the presence of GaN in contact with the QD side facets, which imposes in a uniaxial compressive stress on the dots.

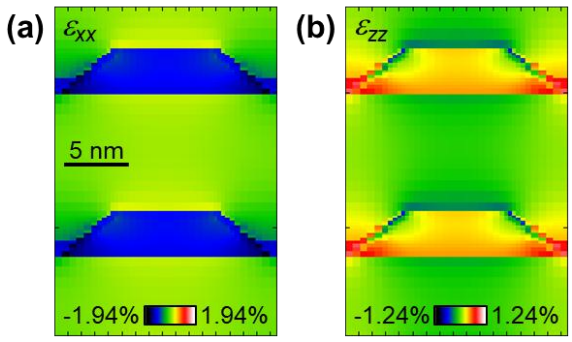

Figure S7. Calculation of the strain distribution in the quantum dots: (a) in-plane strain (ε_{xx}) and (b) out of plane strain (ε_{zz}).

UNIFORMITY OF THE SAMPLE AND REPRODUCIBILITY OF THE RESULTS

PL and CL measurements were performed in several points of the as-grown sample (10×10 mm^2) and we did not observe significant variations in terms of intensity or spectral location of the emission. Then, as a whole, we fabricated with FIB preparation 27 tips, coming from different parts of the sample. The TEM images in figure S3 were taken from a 70-nm-thik lamella specimen processed by FIB. However, it was verified that the results were consistent with TEM images of 11 tips. Eight tips were characterized using *ex-situ* CL. The emission from the dots was systematically observed and its spectral location was consistent with the PL and CL results in the as-grown sample, and with µPL measurements in 3 other tips. Two tips were examined coupling µPL in-situ with La-APT, allowing the identification of the signature of single QDs in the first layers of the stack. Figure 5(a) displays the results from one of the tips, and those of the second tip are shown in figure S8. Precise chemical mapping using La-APT [figure 5(e)] was performed on one tip.

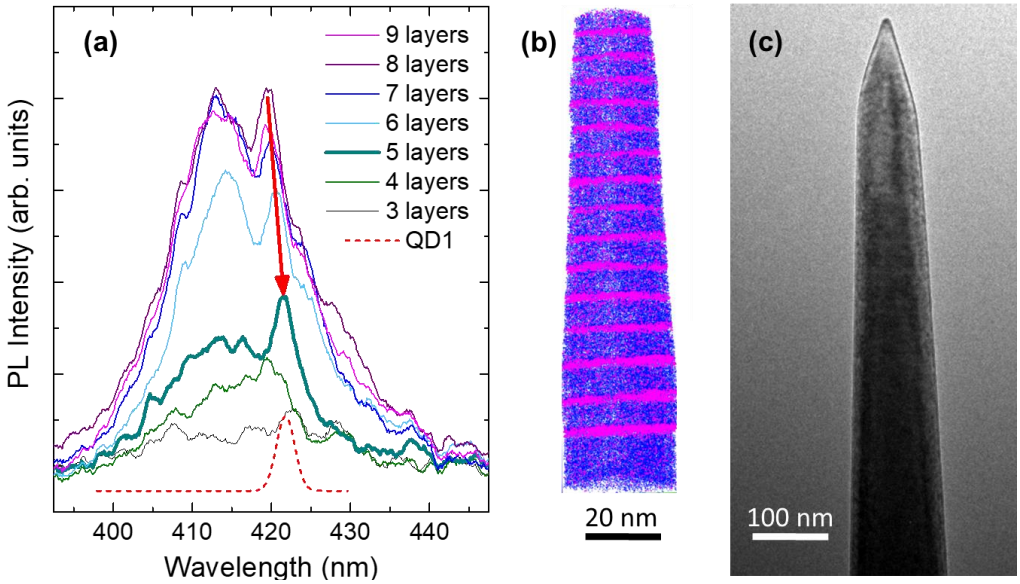

Figure S8. (a) Evolution of the µPL spectrum during the evaporation of the second APT specimen. The spectra represented in the figure were recorded during the evaporation of each barrier. The legend indicates the number of QD layers that were left in the tip. The dashed-line peak is a Lorentzian fit of the emission line that appears in the spectrum labelled "5 layers". Note that this emission red shifted during the evaporation of the tip, as observed for the emission lines from the first specimen [see figures 5(a) and 5(c)]. (b) 3D reconstruction of the In atom distribution in the analysed sample. The APT experiment was performed simultaneously with the µPL measurements. Ga atoms are represented in blue and In atoms are represented in magenta. (c) BF-STEM image of the same tip before being introduced into the APT equipment.

The reproducibility of the measurements and the consistency of the various measurements and calculations confirms the reliability of obtained results and the homogeneity of the sample.

■ AUTHOR INFORMATION

OrcID:
Ioanna Dimkou: 0000-0002-6865-3820
Enrico Di Russo: 0000-0003-3829-6567
Pradip Dalapati: 0000-0001-9021-726X
Jonathan Houard: 0000-0001-7244-205X
Névine Rochat: 0000-0003-3574-4424
David Cooper: 0000-0003-3479-4374
Edith Bellet-Amarlic: 0000-0003-2977-1725
Eva Monroy: 0000-0001-5481-3267
Lorenzo Rigutti: 0000-0001-9141-7706

Present Addresses
[⊥] Current affiliation: UNIROUEN, CNRS, Groupe de Physique des Matériaux, Normandie Université, 76000 Rouen, France

[¶] Current affiliation: Research Center for Nano-Devices and Advanced Materials, Nagoya Institute of Technology, Nagoya 466-8555, Japan